Geochemistry, Geophysics, Geosystems

RESEARCH ARTICLE
10.1029/2020GC009085

Physical Sources of High-Frequency Seismic Noise on Cascadia Initiative Ocean Bottom Seismometers

Rose Hilmo[1] and William S. D. Wilcock[1]

[1]School of Oceanography, University of Washington, Seattle, WA, USA

Key Points:
- Seismic noise is high on the shelf due to wave orbital currents, and noise at the quietest abyssal plain sites is correlated with wind speed
- Ocean currents are the primary source of high-frequency noise on the continental slope and abyssal plain within ~100 km of the slope
- High-frequency current-generated seismic noise is reduced on OBSs with squat hydrodynamic designs and is not clearly reduced by shielding

Supporting Information:
- Supporting Information S1
- Figure S1
- Figure S2

Correspondence to:
R. Hilmo,
wader@uw.edu

Citation:
Hilmo, R., & Wilcock, W. S. D. (2020). Physical sources of high-frequency seismic noise on Cascadia Initiative ocean bottom seismometers. *Geochemistry, Geophysics, Geosystems*, *21*, e2020GC009085. https://doi.org/10.1029/2020GC009085

Received 6 APR 2020
Accepted 21 SEP 2020
Accepted article online 25 SEP 2020

Abstract Physical sources of high-frequency seismic noise in the ocean are investigated using data from the Cascadia Initiative (CI) ocean bottom seismometer (OBS) network, hindcasts of wind speed, waves, and the bottom currents predicted by a regional ocean circulation model and observed at sites on cabled observatories. Seismic data in the 5–12 Hz band are considered because it is best for detecting regional earthquakes and lies between the frequencies of local microseisms and the seasonal whale calls. Median noise levels in this range vary by ~20 dB between sites at a given depth but on average decrease with increasing depth. On the continental shelf, the orbital motions of ocean waves are a major source of noise while at the quietest sites in the deep ocean, noise increases when wind speeds exceed ~10 m/s. On the continental slope and abyssal plain within about 100 km of the slope, seismic noise is not predicted at specific sites by the bottom currents in the ocean circulation model. In these regions, ocean currents are inferred to be the primary source of noise, because noise varies on tidal periods, is low on buried seismometers, and has spatial variations broadly consistent with those of median absolute currents. Comparisons between OBSs suggest that high-frequency noise is reduced by low-profile hydrodynamic designs but not by shielding. Many OBSs also record numerous short duration events on and near the continental shelf that have been attributed elsewhere to animals bumping into the sensor or gas bubbles moving through sediments.

Plain Language Summary Environmental noise generated by waves, wind, and ocean currents limits the ability of seafloor seismometers to detect the ground motions from earthquakes. This research uses data from a large deployment of seafloor seismometers off the coast of the Pacific Northwest of America to understand the seismic noise at frequencies of 5–12 Hz which coincides with the frequency band used to detect regional earthquakes. Instruments deployed in shallow water on the continental shelf record high noise levels caused by motions from ocean waves that reach the seafloor. The quietest sites are found in the deep ocean far from the coast, and here the noise is created by wind blowing spray from whitecaps. At intermediate sites on the continental slope and deep ocean just seaward of the continental slope, the noise results from ocean currents that are related to ocean circulation and tides. Some shallow instruments also record large numbers of short signals that are not earthquakes and may be either a result of animals bumping into the seismic sensor or gas bubbles moving through sediments. The best way to reduce seismic noise is to bury the seismic sensors, but when this is infeasible, the instruments should have a short hydrodynamic design.

1. Introduction

Seismic instruments are distributed unevenly on Earth's surface, primarily because of the presence of oceans where seismic stations are much more difficult and costly to deploy. The resulting gaps in seismic coverage and the location of most tectonic plate boundaries, either within the ocean or near ocean-continent boundaries, have motivated the development of ocean bottom seismometers (OBSs) over the past half a century (Ewing & Ewing, 1961; Francis et al., 1975). Within the academic community, large fleets of OBSs are now available for deployments of a year or more (e.g., Toomey et al., 2014). One of the challenges of seismic observations in the oceans is that environmental noise is generally higher than typical continental settings, primarily because of broadband noise generated by oceanic processes (Webb, 1998). Understanding the sources and amplitudes of seismic noise on in the oceans is important for improving OBS instrument designs and for optimizing the configuration and analysis of OBS experiments.

Microseismic noise in the 0.05 to 1 Hz frequency band is a dominant feature in seismic noise spectra in the oceans and on land (Sutton et al., 1965). There are two microseism peaks which are generated from ocean waves by distinct mechanisms. The primary microseism peak is a small peak from 0.05 to 0.1 Hz that is caused by direct coupling of ocean surface waves with the seafloor in shallow shelf regions (Hasselmann, 1963). Because large ocean swells propagate for long distances throughout the ocean, primary microseisms are generated on most continental margins (Frontera et al., 2010; Webb, 1998). The secondary microseism peak from 0.14 to 0.2 Hz contains by far the most energy and is caused by a nonlinear interaction between surface waves traveling in opposite directions in deep water that results in a doubling of frequency (Ardhuin et al., 2015; Longuet-Higgins, 1950). Microseism noise propagates around the Earth as Rayleigh waves. The microseism peaks are observable on land-based seismometers but can be 20–30 dB higher amplitude on OBSs (Dozorov & Soloviev, 1991). Microseismic noise propagating at higher frequencies attenuates more rapidly with distance, so near the upper limit of the microseismic band (~1 Hz), it is primarily generated locally. The source of this noise is primarily small ocean wind waves. They reach saturation amplitudes at modest wind speeds, which means that noise in this band on OBSs is consistently high. These high noise levels limit detectability of high-frequency teleseismic *P* waves, except during occasional periods of calm when noise levels drop (Webb, 1998; Wilcock et al., 1999).

Because noise levels are high in the microseism band, the most sensitive seismic observations are usually made at lower or higher frequencies. At frequencies <0.03 Hz, the direct pressure signals from ocean infragravity waves dominate noise spectra with increasing amplitudes at longer periods. This leads to a low noise notch between the infragravity noise band and microseismic noise bands on land and in the deep ocean (Dozorov & Soloviev, 1991) that facilitates the recording of body and surface waves from moderately sized teleseismic earthquakes. This noise notch is obscured on shallower OBSs by the pressure signals from higher-frequency ocean waves coupling with the seafloor. However, noise from ocean waves can be reduced on vertical seismometer channels because it is coherent with the tilt noise recorded on horizontal channels or seafloor pressure (Crawford & Webb, 2000).

Noise in the infragravity band is highly variable temporally and spatially, with most energy being generated in shallow coastal areas, resulting in noise levels on vertical channels up to 40 dB higher than on inland sensors (Ardhuin et al., 2015; Frontera et al., 2010; Webb, 1998). Additionally, noise levels on horizontal OBS channels can be up to 40 dB higher than vertical channels due to horizontal tilt caused by infragravity wave loading and motions induced by ocean bottom currents (Pillet et al., 2009; Webb & Crawford, 2010). Current induced noise can be eliminated by installing seafloor instruments in boreholes or burying them in sediments (Montagner et al., 1994; Pillet et al., 2009; Stakes et al., 1998).

The frequency band above microseisms is important for detecting body waves from regional and local earthquakes and is also characterized by generally higher ambient noise levels in the ocean than on land. Microseismic noise from very short period ocean waves dominates spectra up to a few hertz and, because these waves are mostly at saturation amplitudes, leads to a constant noise level that has been termed the "Holu Spectrum" (McCreery et al., 1993). At higher frequencies of 4–30 Hz, the same noise floor is also observed at low wind speeds. As the wind speed increases above a threshold of ~8 m/s, noise levels rise with no observed ceiling which is thought to be due to acoustic noise generated by the spray blowing off whitecaps with a second source near land from surf breaking against the coast (Duennebier et al., 1987; McCreery et al., 1993). Bottom currents are also an important noise source on vertical and horizontal channels. Trehu (1985) found that ground velocity amplitudes measured in the 2–5 Hz band rise as the square of current speeds, once currents exceed 10 cm/s. Comparisons between sensors that are buried in sediments and OBS resting on top of the sediments show that vertical channel short-period noise (>1 Hz) on buried instruments is on average 10 dB quieter than seafloor instruments (Collins et al., 2001; Duennebier & Sutton, 1995). In addition, seafloor OBSs are often poorly coupled leading to much higher noise levels on horizontal channels than the vertical channel, shear wave signals leaking onto the vertical channel due to slight misalignment of the instrument, and peaks in noise at certain frequencies due to instrument resonance with bottom currents (Duennebier & Sutton, 1995; Stähler et al., 2018; Trehu, 1985).

At frequencies above the microseism band, stereotypical impulsive noise signals, termed short duration events (SDEs), which are not earthquakes, have been observed on OBSs worldwide (Batsi et al., 2019; Buskirk et al., 1981). SDEs vary in shape but tend to be characterized by a fairly sharp onset, monotone frequency content, and an exponential decay lasting no more than seconds. Individual SDEs are only recorded on single seismometers even when other instruments are collocated within 1 km, which indicates their source must be near the instrument (Batsi et al., 2019; Tary et al., 2012). SDEs also tend to occur in swarms. SDEs have been reported for at all depths and a range of geographies, although by far the most SDE are recorded in shallow seas and on the continental shelf (Batsi et al., 2019; Buskirk et al., 1981). SDEs have been reported for shallow waters in Deception Island, Antarctica (Bowman & Wilcock, 2014), the Sea of Marmara (Tary et al., 2012), central Chile (Batsi et al., 2019), Kodiak, Alaska, and many other coastal regions (Buskirk et al., 1981). They have also been observed previously on the continental shelf and slope off the coast of Oregon (Williams et al., 2010). SDEs were originally attributed to biological interactions termed "fish-bumps" or "bio-bumps" (Buskirk et al., 1981) but have more recently have been alternatively interpreted as the result of the movement of gas within in seafloor sediments (Batsi et al., 2019; Tary et al., 2012).

In this study, we investigate the environmental sources of seismic noise at frequencies above the microseism band on the vertical channel of OBSs that were deployed off the coast of the Pacific Northwest for the Cascadia Initiative (CI) experiment (FSDN network name 7D) (Toomey et al., 2014). We consider the 5–12 Hz frequency band as representative of frequencies use to detect regional and local earthquakes. We set the upper limit to avoid the seasonal noise of fin and blue whales. The "20 Hz", 1 s fin whale call extends as low as ~14 Hz (Weirathmueller et al., 2017) and the A and B calls of the Northeast Pacific blue whale are centered at ~14 Hz (e.g., Dunn & Hernandez, 2009). We set the lower limit to avoid the effects of local microseism. This was the first large-scale OBS experiment to extend from the continental shelf to the seafloor and thus allows for the investigation of noise levels at different depths and distances from a continental margin. The experiment utilized several different types of OBSs including two new types of shielded OBSs that are designed to protect the OBS from bottom trawling and reduce current generated noise. The experiment footprint also encloses the Ocean Networks Canada (ONC) NEPTUNE cabled observatory (FSDN network name NV) and the Ocean Observatory Initiative (OOI) Cabled Array (FSDN network name OO) which allows for direct comparisons of noise on the buried OBSs on the cabled observatories with the CI OBSs on the seafloor.

2. Methods

2.1. Seismic Data

The CI was a 4-year (2011–2015) deployment of ~70 OBSs off the coast of the Pacific Northwest for the purpose of characterizing the seismicity and imaging the subsurface structure of the Cascadia subduction zone and Juan de Fuca plate (Toomey et al., 2014). The footprint of the experiment extended ~1,000 km along the coast of the Pacific Northwest from Vancouver Island to Cape Mendocino and up to ~400 km offshore with instruments deployed in alternating north and south configurations (Figure 1). Deployment depths varied from ~50 to ~4,000 m, with sites 70 km apart in deep water and as close as a 10 km on the continental slope and shelf in certain areas of interest. In this study, we analyze data from years 3 (2013–2014) and 4 (2014–2015) of the experiment. These deployments covered the entire spatial extent of the experiment and generally have more consistent data quality than the first 2 years.

The experiment used five different broadband OBSs (Figure 2) from the three Instrument Centers in the U.S. Ocean Bottom Seismograph Instrument Pool (OBSIP). Three conventional OBSs were used in water deeper than ~1,000 m, the Woods Hole Oceanographic Institution (WHOI) Keck and ARRA (American Recovery and Reinvestment Act) OBSs (Figures 2a and 2b), and the Lamont Doherty Earth Observatory (LDEO) deep water OBS (Figure 2c). These OBSs include a sensor that is released onto the seafloor from a mechanical arm so that it is decoupled from the main instrument package. Two types of instrument with protective shielding, the Scripps Institution of Oceanography (SIO) Abalones (Figure 2d) and the LDEO trawl-resistant mounts (TRMs) (Figure 2e), were the primary instruments deployed on the continental shelf and upper slope above ~1,000 m depth; the SIO Abalones were also deployed at larger depths, and a few WHOI Keck instruments were deployed at <1,000 m. For both shielded instruments, all the components including the sensor, which is released onto the seafloor, are inside the shielding. The LDEO TRMs have heavy metal shielding for trawl resistance and protection from bottom currents. The SIO Abalones are entirely contained in protective buoyant foam shielding which was designed to shield the seismometer from seafloor currents and provide some

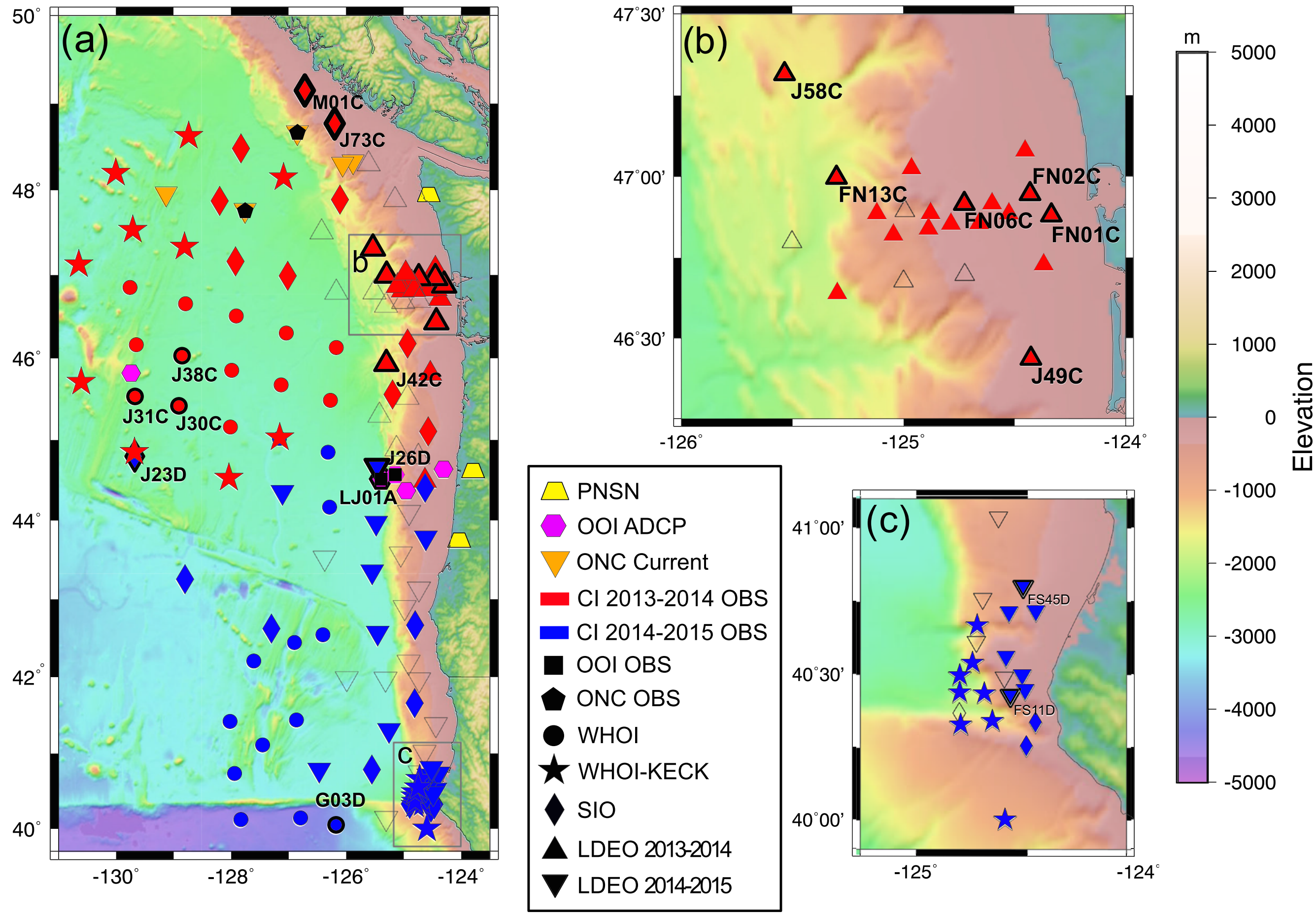

Figure 1. Maps showing the distribution of stations used in this study. Cascadia Initiative (CI) ocean bottom seismometers (OBSs) are shown with the symbol discriminating the instrument type (LDEO triangles (2013–2014 upright, 2014–2015 inverted), WHOI Keck stars, WHOI ARRA circles, SIO Abalone diamonds), color coding indicating the experiment year (red for 2013–14 and blue for 2014–15), and open symbols for instruments with poor quality data that were not used in the analysis. Labeled symbols with bold outlines are used to indicate stations for which examples of data are shown in other figures. Also shown are Ocean Observatories Initiative (OOI) and Ocean Networks Canada (ONC) buried seismometers (black squares and black pentagrams), Pacific Northwest Seismic Network (PNSN) coastal stations (yellow trapezoids), OOI Acoustic Doppler Current Profilers (ADCPs) (pink hexagons), and ONC current meters (orange inverted triangles). Light gray boxes on (a) show the area covered by the maps in (b) and (c) of dense deployments off Grays Harbor and Cape Mendocino, respectively.

trawl resistance. All OBSs employed Nanometrics Trillium Compact seismometers except for the WHOI Keck, which used Gurlap CMG-3T seismometers. Sample rates were 50 Hz for the SIO and WHOI instruments and 125 Hz for the LDEO instruments.

Seismic data from three broadband coastal stations (FORK, BABR, and JEDS) in the Pacific Northwest Seismic Network (PNSN), five stations on the Ocean Observatories Initiative (OOI) cabled array, and two stations on the Ocean Networks Canada (ONC) NEPTUNE cabled observatories were also used for comparison with CI instruments (Figure 1). The ONC instruments and two OOI instruments employ Guralp CMG-1T sensors, and the other three OOI instruments employ Guralp CMG-6TF sensors. Four OOI instruments are located on Hydrate Ridge (~750 m depth) and one at the same latitude at the base of the continental slope (~2,800 m depth). The ONC stations used are on the northern Juan de Fuca plate (site NC27 at ~2,700 m depth) and on the continental slope off of Vancouver Island (site NC89 ~1,250 m depth). The sensors for the cabled stations are buried using a remotely operated vehicle (Romanowicz et al., 2006). The burial of sensors provides better coupling to the seafloor and isolates them from bottom currents (Collins et al., 2001; Duennebier & Sutton, 1995).

10.1029/2020GC009085

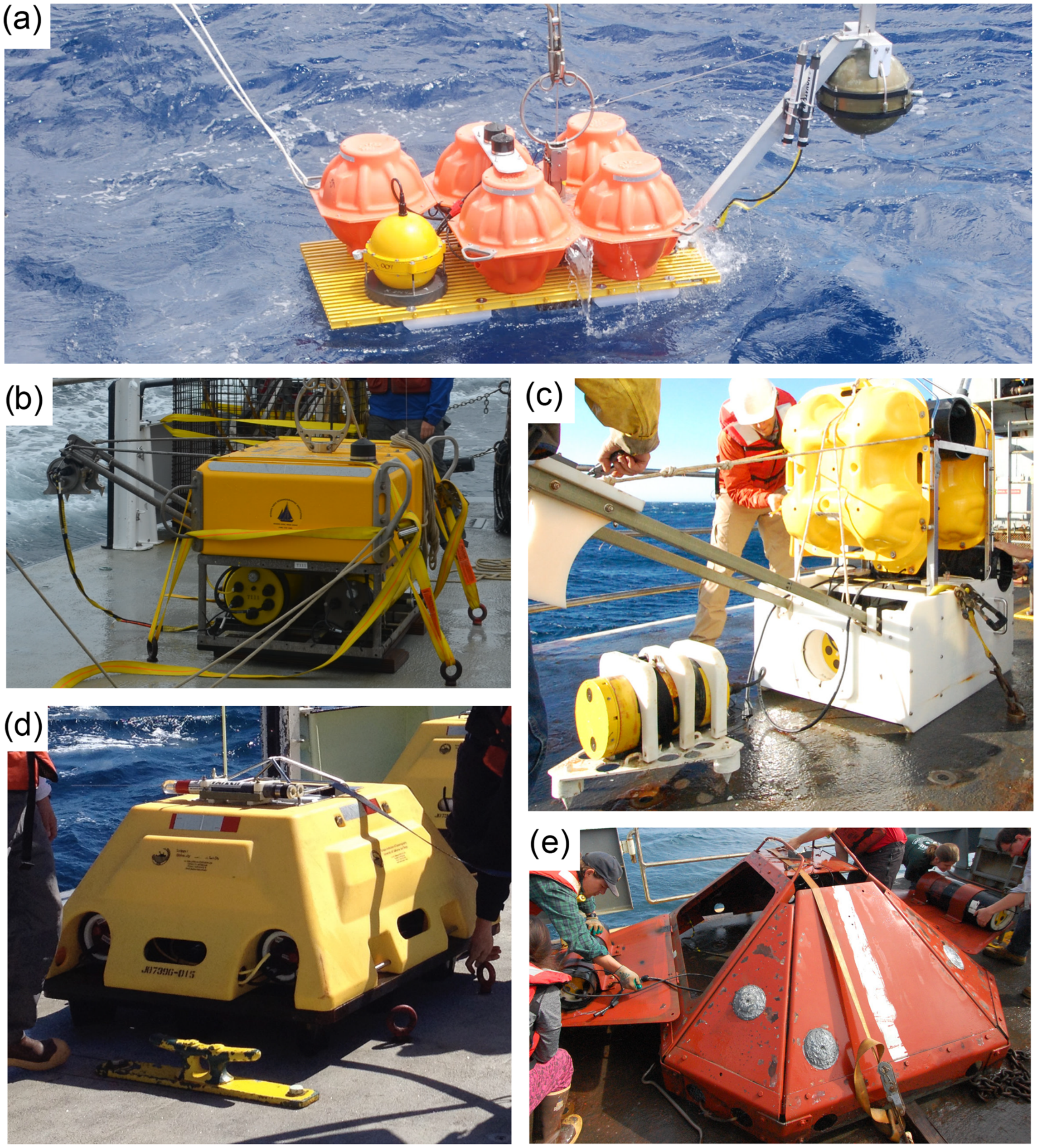

Figure 2. Photographs of ocean bottom seismometers (OBSs) used in the Cascadia Initiative experiment. (a) Woods Hole Oceanographic Institution (WHOI) Keck OBS, (b) WHOI ARRA OBS, (c) Lamont Doherty Earth Institute (LDEO) standard deep OBS, (d) Scripps Institution of Oceanography Abalone OBS, (e) LDEO Trawl Resistant Mount (TRM) OBS. (Photo credits: (a) Jeffrey McGuire, (b) Aubreya Adams, (c) Erik Fredrickson, (d) Douglas Toomey, and (e) Erik Fredrickson).

2.2. Seismic Processing

Vertical component seismic data were downloaded from the Incorporated Research Institutions for Seismology (IRIS) Data Management Center. Any stations marked as poor or bad quality by OBSIP (http://ds.iris.edu/data/reports/7D_2011_2017/) were removed from analysis. In addition, if stations showed noise levels that were orders of magnitude different from nearby sites or had large stereotyped (consistent character and repetitive) signals that appeared instrumental in origin throughout the deployment period, they were also removed from the analysis. If instruments recorded good data for at least 2 months, the bad data were discarded, and the rest kept for analysis.

In an attempt to verify instrument gains, we compared the amplitudes of secondary microseisms between OBSs (see supporting information, Ocean Bottom Seismometer Gains and Figures S3–S4). The results suggest that there may be a gain offset of ~10 dB between the LDEO OBSs in 2013–2014 and 2014–2015 with the gains in 2013–2014 possibly lower than reported. However, since we cannot be certain of this offset, no gain correction is applied to these OBSs. In addition, we inspected the noise spectra of all instruments to search for evidence of poor gains or instrumental noise in the 5–12 Hz frequency band (see supporting information, LDEO OBS Response and Instrument Noise and Figure S5). This led to the elimination of six LDEO stations that were dominated by instrumental noise at 5–12 Hz and one LDEO and one SIO station that had bad gains. In addition, two LDEO TRM OBSs, FS11D and FS45D, were kept in the analysis but may be somewhat impacted by instrumental noise.

In total, 53 and 43 CI stations were used for analysis from the 2013–2014 and 2014–2015 deployments, respectively. One year of data was used for each cabled and land station: ONC data starting 1 September 2014, OOI data starting 1 February 2016, and PNSN data starting 1 January 2015.

To analyze the seismic data, ground velocity timeseries were demeaned for each 2-day segment, and amplitude spectrograms of absolute ground velocity were calculated using 10-min normalized Hanning windows with 50% overlap and then corrected for instrument response. The median power spectral density (PSD) was determined by taking the median value of spectrograms at each frequency.

Median ground velocity amplitudes were used in environmental models to avoid effects of transient and impulsive signals. To examine variations in noise levels in the 5–12 Hz frequency band of interest over time, we computed median noise levels in 10-minute windows. Raw timeseries data were demeaned, and a fourth-order 5–12 Hz Butterworth bandpass filter was applied to extract data. Median absolute values of data in 10-min windows with 50% overlap were calculated and scaled by the average instrument response in the frequency band of interest. Resulting median series used in environmental model were smoothed by convolving with a 48-hr wide Gaussian function normalized to sum to unity to minimize tidal signals and other short-term variations.

To measure the effects of transient/impulse and ambient sources on seismic noise levels in the 5–12 Hz band, we also calculated root-mean squared amplitude values of the same 10-min windows used for medians. The ratio of root-mean squared amplitude values to median values was used to investigate how the relative contributions of transient and continuous noise sources vary temporally and spatially across the CI network.

2.3. Environmental Data and Models

Wind and wave data for 2013–2015 were retrieved from NOAA's Wavewatch III production hindcast (Tolman, 1989, 2006). Hindcast data include hourly wind velocity and bulk spectral estimates for each wave system with a 10 min of arc grid resolution for the U.S. West Coast. These values are modeled using inputs of wind fields at 10 m above the sea surface calculated by the Global Forecast System. Wind speed, wave wavelength, wave period, and wave height information for the dominant wave partition with the most spectral energy were extracted from the hourly hindcast model at each OBS location. Maximum horizontal wave particle velocities, u, at 1 m above the seafloor were determined from wave information using depth-independent linear (Airy) wave equations (Wiegel & Johnson, 1950):

$$u = \frac{\pi h}{T} \frac{\cosh\left[\frac{2\pi(z+d)}{L}\right]}{\sinh\left(\frac{2\pi d}{L}\right)} \tag{1}$$

where h is wave height, T is wave period, d is total depth of the water column (positive value), L is wavelength, and z is vertical position, relative to $z = 0$ at the mean sea surface, of the velocity calculation (negative value).

Modeled hourly bottom currents at 1 m above the seafloor at each OBS site were extracted from the LiveOcean regional oceanographic circulation model (Giddings et al., 2014; MacCready & Giddings, 2016). The model has 40 vertical levels spread between seafloor and sea surface, with tighter spacing near the top and bottom. The finest horizontal resolution is 1.5 km but is closer to 3 km over the region considered here. The model includes realistic forcing of tides and wind and has been shown to simulate well tidally averaged along-shelf currents on the continental shelf (Giddings et al., 2014); however, it has been less well tested on the slope and abyss.

To evaluate the predictions of the circulation model, bottom current data were downloaded for the ONC NEPTUNE and OOI cabled observatories. We considered five ONC stations equipped with bottom current sensors and five OOI stations equipped with acoustic Doppler current profilers (ADCPs) at locations that spanned the continental shelf, slope and abyssal plain (Figure 1). Bottom current measurements were averaged by taking the hourly median absolute value for comparison with noise. ONC bottom current sensors are located ~1 m above the seafloor. The ADCPs measured current velocities at ~10 m above the seafloor, but for comparison were extrapolated to 1 m using the turbulent flow equation for the log layer (Keulegan, 1938):

$$\overline{u} = \frac{u^*}{0.41} \times ln\left(\frac{Z}{z_0}\right) \tag{2}$$

where $\overline{u}$ is the mean (i.e., after averaging over turbulent time scales) current speed, u^* is the friction velocity, Z is the height above the seafloor, and z_0 is the characteristic roughness of the seafloor. We used $z_0 = 0.0007$ m, typical of a uniform mud-sand substrate (Dyer, 1986).

2.4. Modeling Seismic Noise With Environmental Data

Wind and wave data from the NOAA Wavewatch hindcast model and LiveOcean bottom currents from the regional circulation model were investigated as sources of noise on the CI OBSs. The 48-hr smoothed median ground velocities on each instrument were fit with a model as follows:

$$m_t = a + (b_1 + c_1 w_t) + e{v_t}^2 + f{s_t}^2 \quad \text{for } w_t < \mathrm{B} \tag{3a}$$

$$m_t = a + (b_2 + c_2 w_t) + e{v_t}^2 + f{s_t}^2 \quad \text{for } w_t \geq \mathrm{B} \tag{3b}$$

where m is the modeled noise ground velocity, t an index of discretized time, w is wind speed, v is maximum horizontal wave velocity 1 m above the seafloor, s is predicted bottom current, B is the windspeed at the breakpoint for a piecewise linear function with two segments, and the other terms on the right-hand side (a, b_1, b_2, c_1, c_2, e, and f) are constants solved for by regression. In this model, wind speeds are fit with a piecewise function to account for the noise floor observed at lower windspeeds (Duennebier et al., 1987; McCreery et al., 1993), and noise is dependent on the square of wave velocities and bottom current velocities to match the relationship of Trehu (1985). We solved the regression in two steps. We first fit the noise with windspeed to determine the value of B by using a least squared inversion to solve for the two piecewise linear functions with B fixed at values between 5 and 13 m/s spaced at 0.5 m/s intervals and selected the B value resulting in the minimum root mean squared residual. We then used a least squared inversion to solve for all other model parameters. The goodness of fit for our model was determined by calculating R, which compares median ground velocity variance with residual ground velocity variance after model fit is removed:

$$R = 1 - {\sum (g_t - m_t)^2}\Big/{\sum (g_t - mean(g_t))^2} \tag{4}$$

where g_t is the measured ground velocity. Values of R fall between 0 and 1, with the modeled ground velocity, m explaining 100% of variance in the observed ground velocity if $R = 1$ and none of the variance if $R = 0$. The term R is thus the fraction of variance explained by the environmental model.

3. Results

Figure 3 compares the median PSD of CI vertical channel data by depth and instrument type with buried OOI and ONC OBSs and coastal seismometers. Noise in the secondary microseism band is up to ~20 dB higher on CI, ONC, and OOI instruments than coastal instruments. On land-based coastal, deep CI, and deep buried instruments, the primary microseism band is up to ~30 dB quieter than the peak of the secondary microseism band. For CI OBSs shallower than 500 m depth (Figure 3c), the primary microseism peak

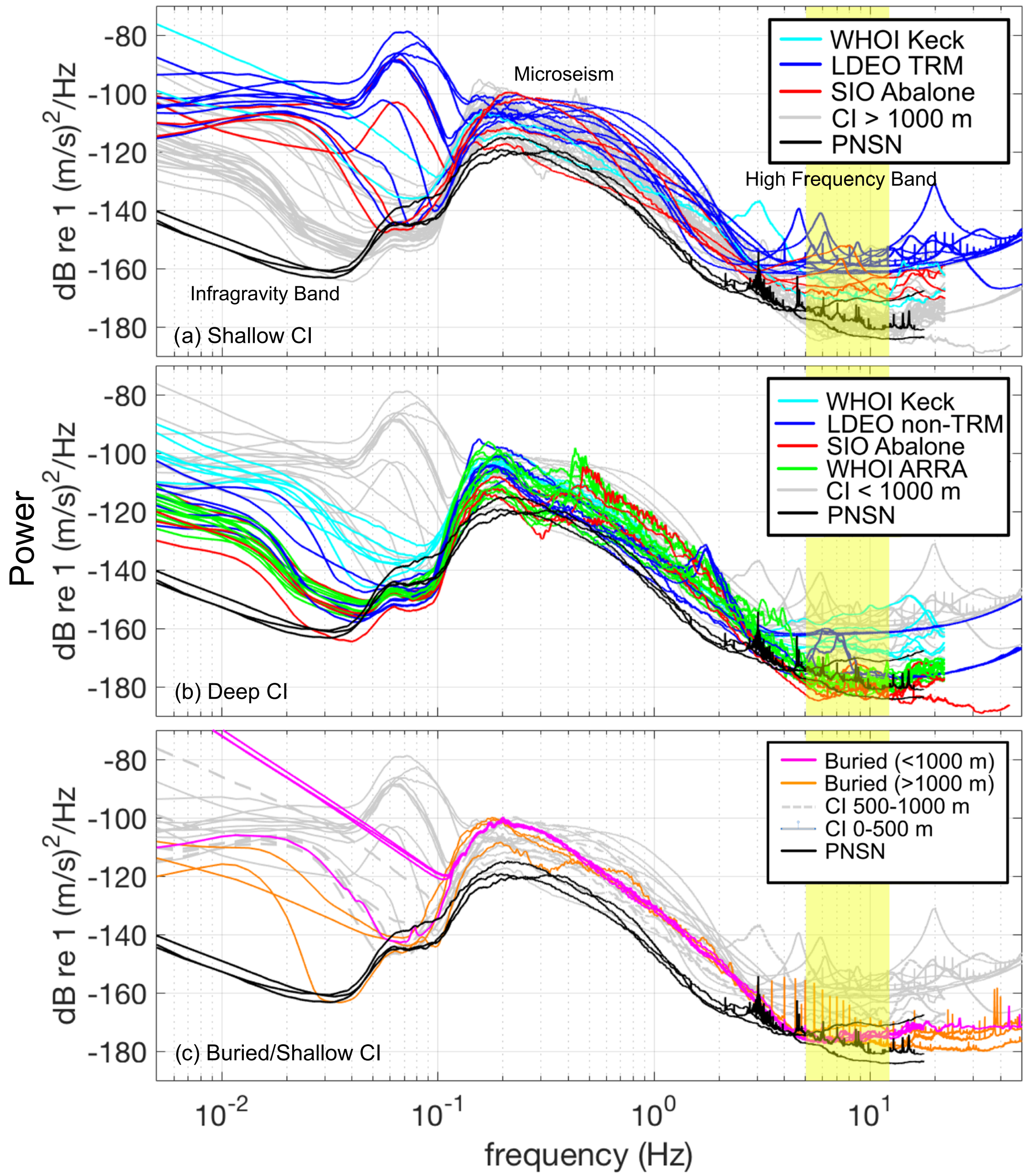

Figure 3. Yearly power spectral density (PSD) plots calculated from medians of spectrograms for the 2014–2015 CI deployment and OOI and ONC buried seismometers, with PNSN coastal seismometers as a reference on each plot (black). (a) Shallow CI stations (<1,000 m) colored by type and deep stations (>1,000 m) in gray. (b) Deep CI stations colored by type and shallow stations in gray. (c) Buried OOI and ONC instruments colored by depth, and shallow CI stations distinguished by depth range (0–500 m dashed gray, 500–1,000 m solid gray). Light yellow shading indicates the 5–12 Hz frequency band that is the focus of this study. Note that in 2014–2015, the spectra for some LDEO instruments at higher frequencies (5 Hz and above) reflect instrumental noise (see supporting information, LDEO OBS Response and Instrument Noise and Figure S5).

exceeds the secondary peak by ~20 dB because the long period ocean swell directly couples with the seabed. As a result, the low-noise notch is completely obscured on shallow stations. Infragravity noise is higher on all OBSs than coastal stations.

In this paper, we consider the 5–12 Hz frequency band as representative of frequencies use to detect regional and local earthquakes. Conventionally, the upper limit of the microseism band is ~1 Hz; however, there is a continuing effect of secondary microseism noise above 1 Hz on deep CI OBSs. For the 1–3 and 3–5 Hz bands,

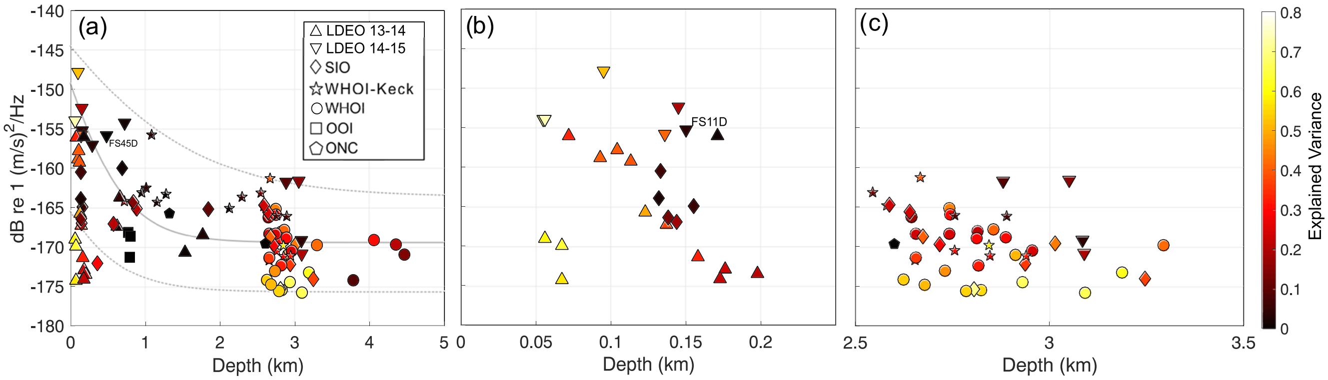

Figure 4. Median yearly noise levels in 5–12 Hz band plotted against depth with color coding to indicate the fraction of variance explained by the model of Equation 3. Instruments types are distinguished by symbol using the conventions of Figure 1 (LDEO triangles, WHOI Keck stars, WHOI ARRA circles, SIO Abalone diamonds, OOI squares, ONC pentagrams). All LDEO instruments <1,000 m depth are TRM and >1,000 m depth are non-TRM. Gray lines show noise levels obtained from the current versus depth functions of Figure 6 obtained using the quadratic relationship (Trehu, 1985) employed in our model and arbitrary scaling. (a) All instruments deployed from 0 to 4,500 m depth. (b) Same as (a) but for stations <250 m deep. (c) Same as (a) but for stations between 2,500 and 3,500 m depth.

microseismic noise levels increase linearly with wind speed up to windspeeds of 12 and 6 m/s, respectively, while in the 5–7 Hz noise levels appear to be essentially constant until spray noise becomes important at windspeeds ≥12 m/s (supporting information Figure S6). Therefore, we choose 5 Hz as the lower frequency limit, above which microseisms contribute to the background noise floor but do not significantly contribute to time dependence.

From the PSD plots, it is clear that noise levels on the CI OBSs in the 5–12 Hz frequency band are strongly variable at all depths but are on average higher on shallow instruments than deep instruments and coastal stations (Figures 3a and 3b). PSD levels of buried OBS are similar at all depths and comparable to coastal stations and the quietest deep CI OBSs (Figure 3c). Many OBSs, especially in shallow water, also show resonance peaks at various frequencies within the 5–12 Hz band that are not present on land and buried sensors.

Noise levels in the 5–12 Hz band are highly variable between CI instruments and are loosely correlated with depth. Variability in ambient noise levels is illustrated by plotting the yearly median absolute values of bandpass filtered timeseries versus instrument depth (Figure 4). These noise levels vary by over 20 dB at any given depth, but in general, there are more shallow stations with high noise levels than deep stations. At depths <200 m the majority of the observations show a decrease in noise levels as depth increases but quite a few LDEO TRMs fall off this trend including three shallow instruments in 2013–2014 with very low noise levels (Figure 4b). In deeper waters the noise levels on the LDEO TRMs (<1,000 m) and LDEO standard OBSs (>1,000 m) are scattered and generally high (Figure 4a). At >2,000 m depth the WHOI ARRA and all but one SIO Abalone have low noise levels compared to most of the WHOI Keck instruments (Figure 4c). The buried OOI and ONC seismometers have similar noise levels at all depths, matching the average for WHOI ARRA and SIO OBSs at >2,000 m depth, but are noticeably quieter than WHOI Keck, SIO, and LDEO OBSs at depths near 1,000 m.

To investigate environmental sources of ambient noise we fit each hourly median ground velocity time series with the model of Equation 3. We found that the bottom currents predicted by the LiveOcean regional oceanographic circulation model did not contribute significantly to the fit to the data (maximum fraction of explained variance <0.08), so we excluded the final term in Equation 3 in the final models. For the deepest stations, ground velocities as a function of windspeed are generally predicted well by the piecewise linear function with a breakpoint (the intersection between the two lines) that is always between 8 and 12 m/s (supporting information Figure S7a) consistent with the findings of McCreery et al. (1993). For stations at <~125 m depth, noise levels are proportional to the square of the maximum particle speeds from ocean waves that propagate deep enough to interact with the seafloor (supporting information Figure S7b) consistent with Trehu (1985). Figure 5 shows examples of median ground velocity timeseries and the model predictions. For the example shallow station at 67 m depth (Figure 5a), the noise is modeled well by a

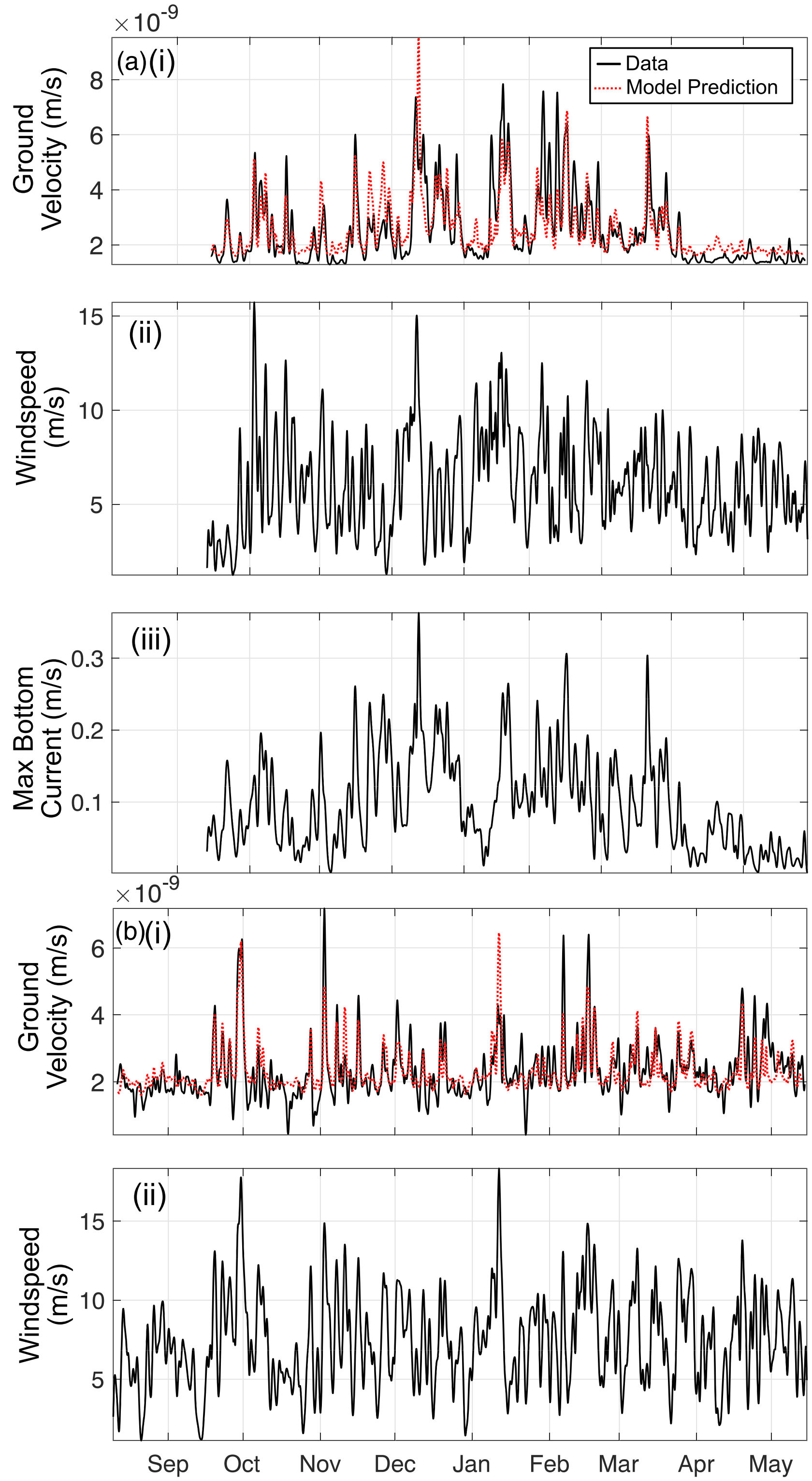

Figure 5. Forty-eight-hour smoothed median noise levels in the 5–12 Hz band (black) and predicted noise levels (red) modeled using environmental parameters (black). (a)(i) Shallow station FN02C, modeled using (ii) wind speed and (iii) maximum wave velocity 1 m above the sea floor. (b)(i) Deep station J31C, modeled using (ii) wind speed only. Station locations are shown in Figure 1.

10.1029/2020GC009085

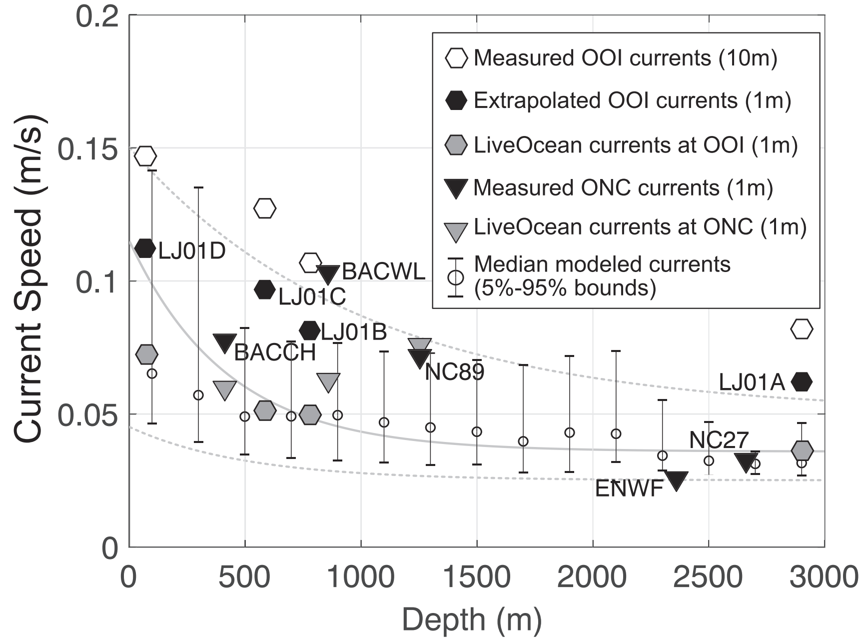

Figure 6. Predicted and observed median absolute ocean bottom currents as a function of depth showing modeled current speeds for the LiveOcean Regional Ocean Modeling circulation model averaged in 200-m bins at 1 m above the seafloor (open circles for the median absolute current and error bars for the 5–95% limits), median absolute currents measured 1 m above the seafloor at ONC cabled stations (black inverted triangles), median absolute currents measured 10 m above the seafloor at OOI ADCP stations (open hexagons) extrapolated to 1 m above the seafloor using the turbulent flow log layer equation (Equation 2) (black hexagons), and modeled currents at 1 m above the seafloor for each ONC and OOI station that lies within the footprint of the model (gray symbols). The center gray line (solid) is a logarithmic function fit to the modeled data. The dashed gray lines are logarithmic curves estimated because they approximately bound the observed and modeled current data.

combination of wave bottom particle velocity and windspeed, yielding a fraction of explained variance of 0.54 that almost entirely comes from the excellent correlation in peaks in noise and wave particle velocity. For a deep station at 2,624 m depth (Figure 5b), the noise is predicted well by only the wind speed yielding a fraction of explained variance of 0.61.

The fraction of variance explained by the model (R) for all CI OBSs is shown by the color scale in Figure 4. The fraction of explained variance varies considerably from near zero to ~0.8 with the largest values on stations shallower than 150 m and deeper than 2.5 km. At depths <200 m, there is a clear tendency for the fraction of explained variance to decrease with increasing depth (Figure 4b). For depths >2.5 km, the quiet WHOI ARRA and SIO Abalone stations with noise levels <170 dB re 1 $(m/s)^2$/Hz have markedly higher fractions of explained variance than the noisier LDEO and WHOI Keck stations. For stations between depths of 150 m and 2.5 km, the model explains very little of the variance.

LiveOcean model bottom current predictions do not explain OBS noise well in our model, but previous research has found that bottom currents are a significant source of noise on OBSs (Trehu, 1985). We compared predictions with actual bottom current measurements (Figure 6) and found the LiveOcean model does not predict bottom currents accurately. This model is designed to model oceanographic circulation on the continental shelf, and its performance at depth has not been validated. However, the LiveOcean model may be adequate to statistically reproduce some patterns in regional bottom currents. To investigate this, we looked at the variability of median predicted bottom current speeds within 200 m depth bins and compared predicted medians with observations at sites on the OOI and ONC cabled observatories (Figure 6). The modeled currents are quite variable in all depth bins particularly at depths <400 m. The average modeled and measured bottom current speeds both decrease with depth but for depths <1,200 m, the modeled current speeds are much lower than measured speeds. The measured median currents at all three sites on the upper continental slope (500–1,000 m) depth are higher than the 95th percentile of the model.

10.1029/2020GC009085

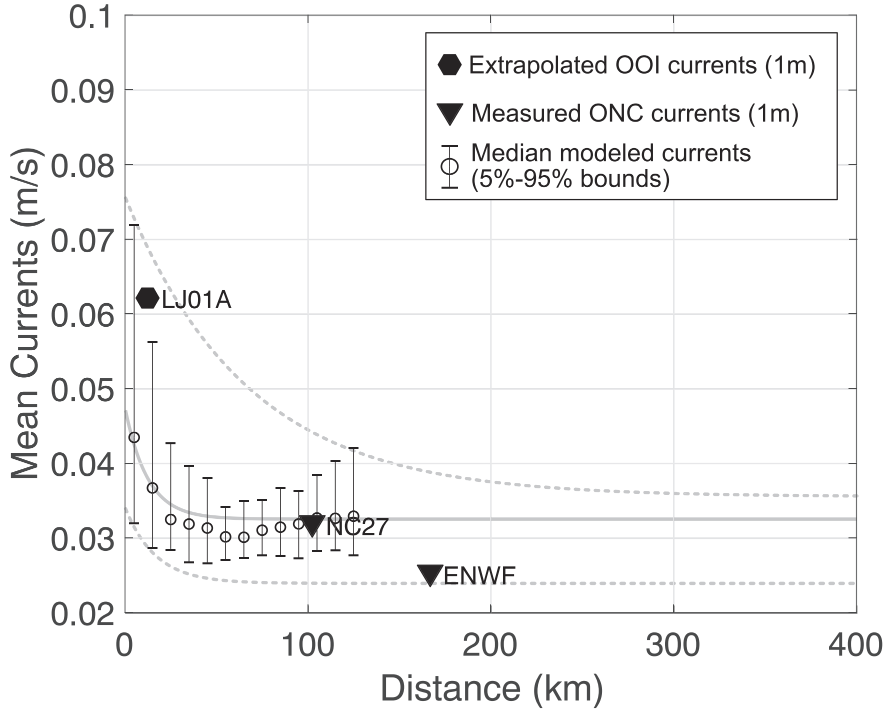

Figure 7. Predicted and observed ocean bottom currents as a function of distance offshore from the 1,800 m contour as a proxy for distance from the base of the continental slope with plotting conventions as for Figure 6. Modeled currents at specific stations are not shown because the ONC seismometers are outside the footprint of the LiveOcean model. The center gray line (solid) is a logarithmic function fit to the modeled data. The dashed gray lines are logarithmic curves estimated because they approximately bound the observed and modeled current data.

Trehu (1985) inferred a current threshold of 10 cm/s for significant current-generated noise in the 2–5 Hz, but this is likely to be lower at higher frequencies where the microseism noise floor is lower. Since the median observed current speeds at shelf and upper slope sites approach ~10 cm/s, we infer that currents on the continental shelf and slope are sufficient to increase noise on CI OBSs, at least during time periods of higher than average currents.

On the abyssal plain the predicted and observed median currents match at two ONC sites (ENWF and NC27) but not at OOI site LJ01A, where measured currents are much higher than predicted. Site LJ01A differs from the ONC sites in that it lies very close to the slope base (Figure 1a). Figure 7 shows predicted and measured abyssal bottom current speeds versus distance from the base of the continental slope. Both modeled and measured bottom current speeds increase approaching the base of the continental slope. Based on the single observation from station LJ01A predictions may be too low near the slope. To evaluate whether ocean currents in this region may be related to noise on OBSs in our frequency band of interest, we plotted median noise levels against station distance from the base of the continental slope as approximated by the 1,800 m contour (Figure 8). Trends in noise reflect trends in bottom currents. Within ~50–100 km of the continental slope, noise levels increase markedly. Stations within 75 km of the slope are on average ~10 dB noisier than those >250 km away with the highest noise levels observed on LDEO non-TRM and WHOI Keck OBSs. Near-slope OBSs are also less well fit by windspeed compared with stations further offshore (Figure 8), consistent with currents generating noise in this region.

Additionally, we inspected spectra of hourly median noise times series for evidence of noise from tidally induced currents. Diurnal and semidiurnal tides have periods of ~24.8 and ~12.4 hr, respectively, that may be halved if currents are symmetric since current speeds will peak during flood and ebb. About half the stations show clear evidence of tidal peaks, and these are predominately sites on the continental shelf and slope or deep sites near the slope or other bathymetric features such as mid-ocean ridges (supporting information Figure S8).

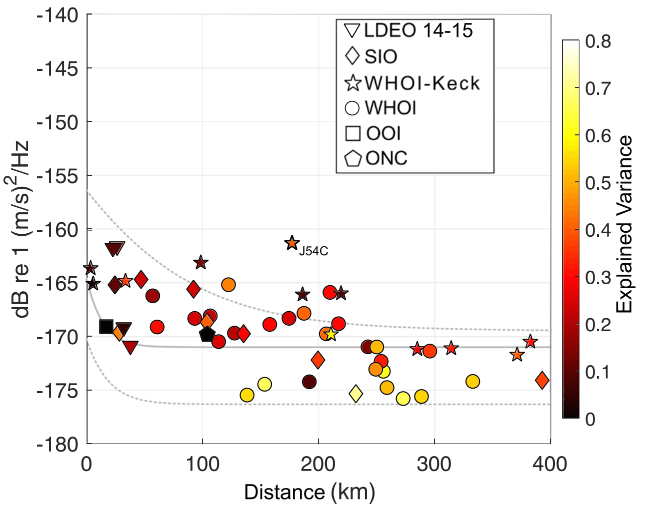

Figure 8. Median yearly noise levels in 5–12 Hz band plotted against distance offshore from the approximate location of the base of the continental slope was represented by the 1,800 m contour using the same conventions as Figure 4. All LDEO stations at these depths are non-TRM. Gray symbols indicate buried cabled seismometers. Gray lines show noise levels obtained from the current versus depth functions of Figure 7 obtained using the quadratic relationship (Trehu, 1985) employed in our model and arbitrary scaling.

To understand if noise is influenced by impulsive versus ambient noise sources, we examined time series of the ratio of noise calculated from hourly rms noise calculations (which are sensitive to transient signals) and hourly median calculations (which are not sensitive to transient signals) in the time domain. Since the former is sensitive to repetitive impulsive noise sources that last for more than half of any given hour, an elevated ratio indicates impulsive sources of noise. Average OBSs with low impulsive noise have a mean to median ratio of ~1.5. Many stations on the continental shelf show large variations in ratios of impulsive noise over time in a variety of patterns. Several shelf stations show a steadily increasing mean to median ratio over the course of the entire deployment (supporting information Figures S9e–S9f). Some have consistently high impulsive noise throughout the deployment (supporting information Figure S9b). Others show episodic or possibly seasonal increased in the mean to median ratio (supporting information Figure S9a, S9c, S9d, S9g, and S9h). One notable episodic occurrence is a 3-week increase in the ratio in May 2014 (supporting information Figure S9h) on both some shallow stations and on deep stations on near the southern Juan de Fuca ridge (blue circles in Figures 9a–9b). An inspection of timeseries shows that the noise source is a swarm of T-phases. An effort to locate events suggests a source well outside the network to the west of the Juan de Fuca Ridge.

For stations on and near the continental shelf, high average mean to median noise ratios are observed on about half the OBSs (Figure 9). An inspection of waveforms shows that except for the T-phase swarm in May 2014, the intermittent noise source is a stereotypical signal that is about 0.5–1 s in length with a relatively sharp onset, a monotone frequency, and an approximately exponential decay of amplitude (Figure 10a). These signals mostly occur as trains of very similar events with variable spacings of a few seconds (Figure 10b). Comparison of the timing of SDEs on closely spaced stations off Grays Harbor and Cape Mendocino shows that each individual event is only recorded on a single station. The signals are also not observed on the pressure sensor, suggesting that that they are generated very close to or on the seismic sensor, or are a seismic phase that does not couple well into the water column.

4. Discussion

4.1. Environmental Sources of Noise

Our empirical model of environmental noise sources in the 5–12 Hz band on CI OBSs successfully explains noise variations on deep instruments well offshore and most very shallow instruments and on the shelf. On deep, quiet OBSs, absolute ground velocities are modeled well by a noise source from wind generated whitecaps at higher wind speeds (McCreery et al., 1993) with wind typically explaining 0.5–0.7 of the noise variance for the quietest WHOI Keck and SIO instruments (Figures 4a) and >0.25 for all but two instruments at least 100 km from the base of the continental shelf (Figure 8). For shallow instruments on the shelf (Figure 4b), there are five instruments, all at depth exceeding 130 m, where wave particle motions do not explain noise variations but the remainder show a very clear trend in which the fraction of explained variance from ocean wave particle motions is high at shallow depths (between 0.6–0.8 at 50–70 m) and decreases with depth (~0.2 at 150–200 m). The median noise levels on the majority of the shallow instruments are also consistent with a trend of decreasing noise levels with depth that might be expected given that the speed of wave particle motions decreases with depth. However, quite a few instruments fall off this trend including three LDEO OBSs at depths of 50–70 m with very low noise levels. The LDEO OBS in 2013–2014 may have gains that are 10 dB lower than reported (see supporting information, Ocean Bottom Seismometer Gains and Figures S3–S4) but applying a +10 dB adjustment to the 2013–2014 LDEO TRMs would still leave these three OBSs well below the trend.

The noise variations on OBSs on the continental slope (Figure 4a) and on the abyssal plain near the base of the slope (Figure 8) are not fit well by the empirical model. We infer that in this region, bottom currents are

10.1029/2020GC009085

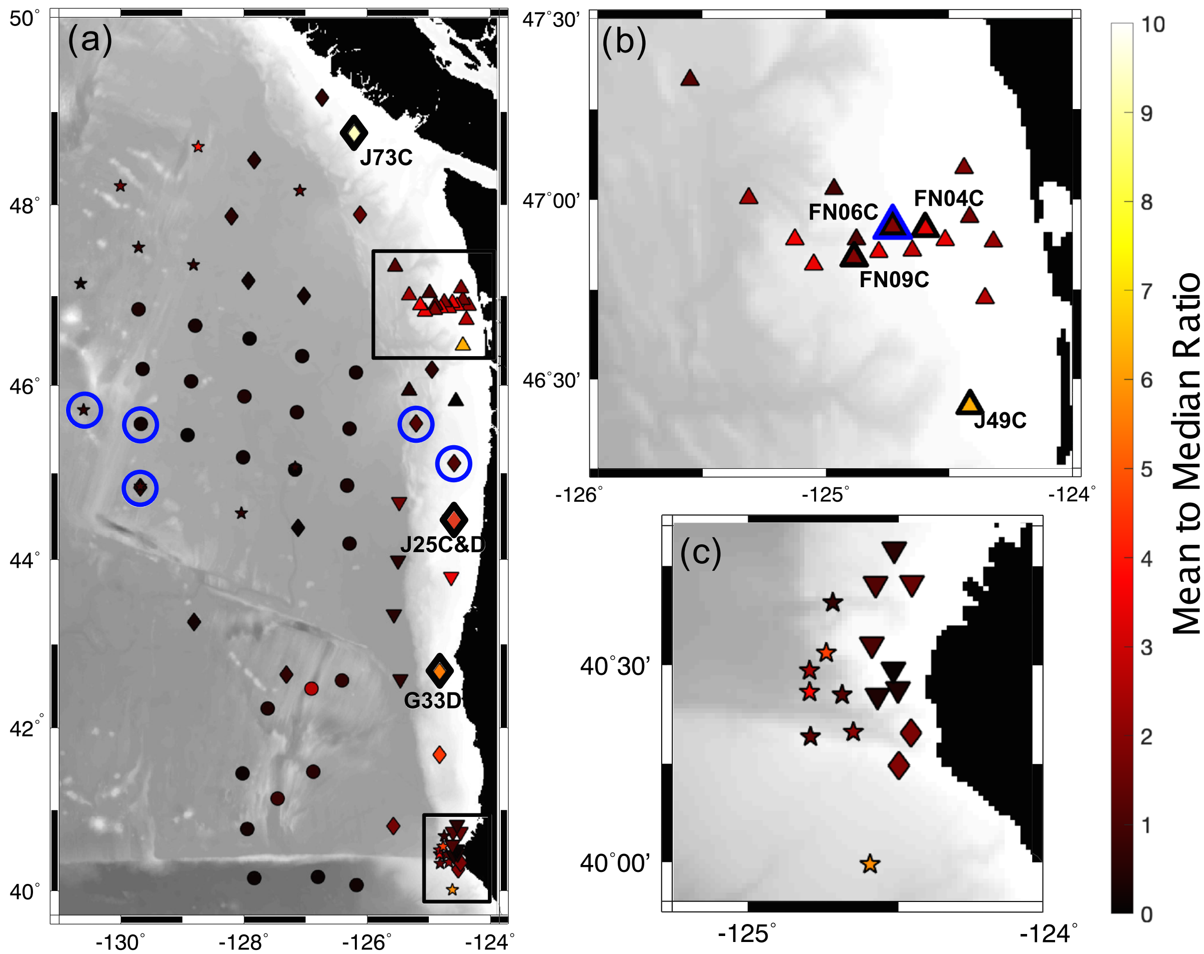

Figure 9. Map of CI OBSs plotted using the conventions of Figures 1a–1c (LDEO circles, WHOI Keck stars, WHOI ARRA triangles, SIO Abalone diamonds) except the colors of station markers indicates mean to median noise ratios. Blue circles indicate stations where a large T-phase swarm in May of 2014 clearly elevated this ratio.

the dominant source of noise. However, the LiveOcean model does not accurately predict temporal variations in bottom current generated noise at any given location. As noted above, the LiveOcean model is designed for modeling circulation on the continental shelf, and it has not been validated with abyssal currents. The LiveOcean model has limited resolution for modeling the effects of bathymetry, and it is modeling processes that are complex and partially chaotic (Csanady, 1988; Yttervik & Furnes, 2005). One notable source of currents that is absent from the model forcing is internal tides coming from the open ocean boundary (Alford et al., 2012), and this lack may explain why currents in the model are weaker than generally observed at sites on the cabled observatories (Figure 6).

On the continental slope, the LiveOcean model predicts that median currents increase as the depth decreases and that there are very large spatial variations in median currents at depths less than 400 m (Figure 6). Observations of currents on the cabled observatories suggest that the LiveOcean model underpredicts currents on the continental slope (Figure 6). On Figure 6, we show three logarithmic relationships between current speed and depth; the functional form is unimportant, but they were chosen so that one approximately fits the observed currents, and the other two approximately bound the observations and match the variability in the LiveOcean predictions at shallow depths. When converted to empirically predicted noise levels using the quadratic relationship of Trehu (1985) at an arbitrary scaling, these yield relationships between current speed and depth that are generally consistent with the trends in noise levels with depth and their variability (Figure 4). Thus, we infer the noise levels on the continental slope are consistent with noise from ocean currents.

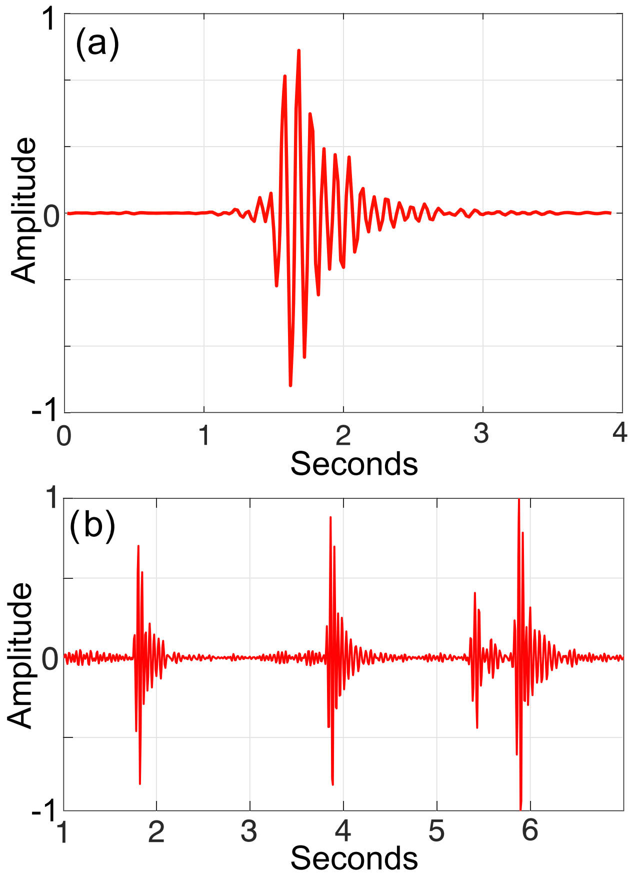

Figure 10. Examples of (a) a single short stereotyped signal and (b) a train of signals on station J73C of the type that are responsible for elevated noise levels on many stations on or near the continental shelf. The station location is shown in Figure 1.

When comparing different deep instruments, the noise on CI OBSs is generally highest near the base of the continental slope and the fit of our model poorest (Figure 8). Similarly, the LiveOcean model predicts higher average median currents and larger spatial variation in median currents at sites within a few tens of kilometers of the slope base (Figure 7). This is supported by observations at the OOI Cabled Array slope base current meter site (station LJ01A in Figure 7) and two ONC sites further from the slope. However, these observations also suggest that the LiveOcean underpredicts currents near the base of the slope. In Figure 7, we also show logarithmic relationships between current speed and distance from the base of the continental slope chosen to approximately match the three observations and enclose the variability predicted by the LiveOcean model. When converted to predicted noise levels using the quadratic relationship of Trehu (1985) they yield relationships that are generally consistent with the trends in noise levels and variability with distance from the base of the continental slope (Figure 8). We infer that the noise patterns in this region reflect the effects of currents on the abyssal plain increasing substantially approaching the base of the continental slope.

We attribute the noise on OBSs on and just seaward of the continental slope to bottom currents from tides, regional bottom currents, and internal waves. We observe variations in noise at tidal frequencies on most slope and near-slope deep OBSs (supporting information Figure S8), and this is most easily explained by tidal currents. Tidal currents not only affect shallow, near-shore stations, but also stations along and near the continental slope through the breaking of internal tides against the slope (Xie et al., 2018). These breaking internal tides have been observed to generate along and across slope currents greater than 10 cm/s. The breaking of internal tidal waves on the continental slope is not the only known cause of high-speed bottom current events at middle depths. Internal solitary waves and wave trains also break against continental slopes and cause turbulent currents up to dozens of cm/s (Boegman & Stastna, 2019). These waves are less common and less predictable than tides; however, they may still be an occasional source of noise on OBSs. Wind and internal wave events can trigger bottom-intensified currents that exceed 10 cm/s for days at a time on the continental slope and deep sea close to continental margins (Csanady, 1988; Yttervik & Furnes, 2005). Also, regional deep ocean currents that are normally <6 cm/s are occasionally intensified up to 15 cm/s by benthic storms (Juan et al., 2018). These regional bottom currents can also be intensified and channeled by topographical barriers including continental slopes which can greatly increase current speeds along the base of the slope (Hayes, 1980). Together these sources of ocean currents not only explain high noise levels and poor model fit on mid depth CI OBSs, but also high noise levels and poor model fit for deep CI OBSs near the continental slope (Figure 8). Noise on OBSs is not only related to the depth of deployment, but also to proximity to large variations in bathymetry.

4.2. Instrument Performance

It also appears that performance differs between OBS designs and that some of the scatter in noise levels is instrumental. Although we have made an effort to eliminate individual instruments with incorrect gains by comparing the amplitudes of microseisms (see supporting information, Ocean Bottom Seismometer Gains and Figures S3–S4), this approach has limited precision because of the scatter in microseism amplitudes and so some offsets in gains may persist. For example, deep WHOI station J54C may have a gain that is too high; it is at 2,700 m depth lies 180 km away from the base of the continental slope and has noise levels markedly higher than all other instruments a similar distance offshore (Figure 8) even though the wind explains a fraction of 0.44 of the variance.

10.1029/2020GC009085

As discussed in the supporting information, there is also uncertainty in the gains of the LDEO OBSs with the possibility that the gains of the LDEO instruments in 2013–2014 may be 10 dB too low relative to the LDEO instruments in 2014–2015 and other instruments. Without gain adjustments, noise levels on the OBSs at <100 m depth, which are all LDEO TRMs, vary by over 25 dB, and the noise levels are not correlated with how well they are fit by the empirical model (Figure 4b). Applying a correction to relative gains between 2013–2014 and 2014–2015 would reduce the variation to 15 dB. High noise levels may be explained by poor coupling of an instrument to the seafloor leading to rocking of the instrument due to ocean waves. However, it is more difficult to explain very quiet shallow stations with noise levels that are similar to deep stations on the abyssal plain. Without a gain adjustment, the median noise levels on the three quietest shallow TRMs at 50–70 m depth are comparable to the quietest deep water OBSs. If noise levels were really this low, we would expect the empirical model to reveal a noise source consistent with wind generated spray which it does not. These observations are most simply explained if the gains are wrong. However, if a gain adjustment is applied to all 2013–2014 LDEO OBSs there would still be a 10–15 dB offset between the gains of the three anomalous shallow instruments and other nosier 2013–2014 LDEO TRMs at ~100 m depth. This is difficult to explain based on the expectations of noise from wave motions unless the gains vary between LDEO TRMS vary in the 5–12 Hz band.

Variations in noise levels with respect to instrument type at different depths appear complex due to large scatter in noise levels at any given depth and the different mix of stations at different depths (Figure 4). On the continental slope and abyssal plain (Figures 4a and 8), the WHOI Keck instruments tend to be ~5–10 dB noisier than the SIO and WHOI ARRA OBSs. The quietest deep instruments are mostly WHOI ARRA OBSs with the SIO OBS ~5 dB noisier (Figure 4a). However, when examined as a function of distance from the base of continental slope the differences are more muted with the noise levels on WHOI ARRA and SIO OBSs in equivalent positions quite similar. The LDEO TRMs on the upper continental slope (200–1,000 m) are nosier than the SIO OBSs at similar depths and WHOI Keck OBSs at somewhat greater depths. Only a few LDEO non-TRMs from 2014 to 2015 are located deeper than 1,800 m, and they have relatively high noise levels (Figure 4a) but their noise levels while more variable are comparable on average to SIO and WHOI ARRA instruments at similar distances from the continental shelf.

Although there is some uncertainty with the LDEO instrument gains, it seems likely that the differing instrument designs may result in differences in turbulent generation of noise by bottom currents. This is supported by the presence of resonance peaks at in PSD plots (Figure 3). Peaks in noise at various frequencies have been observed previously to be the result of large instrument packages resonating with local sediment structure. These resonances are generated locally and are highly dependent on how bottom currents interact with instrument packages (Godin & Chapman, 1999; Trehu & Sutton, 1994). LDEO non-TRM instrument platforms are taller than all other instrument designs (Figure 2c). In the log-layer where currents are affected by friction interaction with the seafloor, bottom boundary current velocities increase logarithmically away from the seafloor (Keulegan, 1938), so taller instruments will be subjected to higher currents and increased turbulence. The WHOI Keck instrument platforms are very rough with multiple floats arrayed horizontally on a platform (Figure 2a) which will also increase the generation of turbulent eddies. The Gurlap CMG-3T sensor used on the WHOI Keck OBS is spherical and at lower frequencies has been observed to be less well coupled to the seafloor than cylindrical Nanometrics Trillium Compact seismometers with tripod feet on the other instruments, resulting in bleed over from horizontal channels onto the vertical (Bell et al., 2015). Poor coupling of the Gurlap CMG-3T sensor package may also increase noise at higher frequencies and its larger size that may lead to more high-frequency noise generated by turbulence. Compared to WHOI Keck and LDEO non-TRMs, the WHOI ARRA and SIO Abalone instrument are relatively compact and have smooth hydrodynamic profiles.

It is also important to consider whether shielding limits high-frequency current generated noise. On the abyssal plain near the base of continental slope where there is good evidence that currents dominate the noise, the WHOI ARRA and SIO Abalone instruments have similar noise levels (Figure 8). This suggests that the shielding on SIO Abalones does not reduce current generated noise compared to the unshielded WHOI ARRA instruments. Additionally, on the outer shelf and upper slope, the noise levels tend to be higher on the bulky LDEO TRMs than on SIO Abalones which may indicate that higher noise is associated with larger housings regardless of shielding. Bulky instrument housings in very close proximity to the sensor are likely

10.1029/2020GC009085

to be prone to the same resonance peaks as instrument packages, which may explain the especially prominent resonance peaks in PSD plots for LDEO TRM OBSs (Figure 3a).

In summary, noise levels appear to vary between instruments primarily because of differences in hydrodynamic profiles. The quietest instruments are the WHOI ARRA and SIO Abalone instruments due to their low height and relatively smooth profiles. Shielding on shallow instruments has been an effective way to reduce noise on OBSs for low-frequency seismic studies (Bell et al., 2015) but does not seem to lower noise levels in the 5–12 Hz band used in our study, although the comparisons between shielded and unshielded instruments would be more robust if unshielded instruments were deployed in shallow water. The most effective way to remove the effects of bottom current and wave generated currents on OBSs would be to bury them in sediments in a similar way to OOI and ONC stations. However, because burying instruments is not presently feasible for autonomous OBSs networks, it may be more practical to design instrument platforms and shields to have low profile and hydrodynamic shapes so as to minimize noise from turbulence generated by current interactions with the instruments. Ideally, instruments designed to minimize current generated noise should be deployed near a seafloor current meter to directly evaluate their performance.

4.3. Impulsive Signals

Many of the instruments on and near the continental shelf are characterized by a high average ratio of root mean squared to median noise levels. This ratio, which we term the “mean to median ratio,” will increase during periods when intermittent noise sources are present for more than half of 1 hr. Inspection of time series shows that, with the exception of a T-phase swarm in May 2014, the source of the noise is repeated stereotyped signals that tend to last less than a second with a fairly sharp onset, monotone frequency content, and exponential decay (Figure 10). Very similar signals have been identified in several previous studies and have been termed short duration events (SDEs) (Batsi et al., 2019).

Average values of the mean to median ratio exceed 7 on a few stations and are >4 on about half the stations on the continental shelf (Figure 9) compared with values of about 1.5 on most deep stations when SDEs are not common. Thus, it appears that SDEs are the dominant source of high-frequency impulsive noise on many OBSs on the continental shelf. Values of the mean to median ratio can vary substantially between closely spaced stations, and stations with the highest mean to median ratios are scattered across the Cascadia shelf (Figures 9b and 9c). Of the two stations on the shelf off the coast on Vancouver Island, one has the highest value observed, and the other is only slightly elevated (Figure 9a). The mean to median ratio is on average higher off Grays Harbor than Cape Mendocino. Between these two areas of dense OBS deployments, the ratio is much higher on the three continental shelf stations south of 44°N than stations further north. The geographical scatter apparent in where SDEs are recorded indicates that their source is likely a process that is localized to each instrument.

SDEs were originally attributed to biological interactions termed “fish-bumps” or “bio-bumps” (Buskirk et al., 1981), but may instead be explained by movement of gas within in seafloor sediments (Batsi et al., 2019; Tary et al., 2012). Both of these mechanisms occur proximally to the instrument, which is consistent with the observation that individual SDEs are only observed on single stations. They are also consistent with observations that the signals are not observed on collocated pressure sensors. A bio-bump would only affect the sensor the animal touched. If gas-related motions occur very close to the seismic sensor or generate primarily shear waves, they would be hard to detect on a hydrophone or pressure gauge (Tary et al., 2012). Buskirk noted that the rate of SDEs varied diurnally and argued that this was consistent with a biological origin. Tary et al. (2012) argued for a gas-related mechanism because they observed that some large SDEs in the Sea of Marmara were also present on the pressure sensor. Based on correlating camera observations with seismic recordings at a single sensor in 15 m of water offshore Brittany, Batsi et al. (2019) also concluded that fish-bumps were not responsible for SDEs.

In our study, there is a tendency for the intensity of SDE noise on some continental shelf OBSs, as measured by the mean to median ratio, to increase throughout the deployment (supporting information Figures S9c and S9e–S9g). This could be due to increasing biological interaction over time as seafloor animals find and colonize the OBSs. Fish were commonly observed nearby or within shallow instrument shields by cameras during the recovery of the instruments (supporting information Figure S10a). Additionally, sea anemones, snail eggs, and basket stars were often found attached to the instrument shielding upon retrieval

10.1029/2020GC009085

of CI OBSs (supporting information Figure S10b). Some shelf OBSs also showed episodic increases in SDE noise and variations consistent with a seasonal cycle (supporting information Figures S9a, S9c–S9d, and S9f–S9g) that might be linked to the lifecycles of animals. Alternatively, the episodic patterns in SDEs may be associated with varying intensities of gas bubble activity and seasonal variations may be regulated by pressure changes from spring upwelling off the Pacific Northwest coast and seasonal changes in bottom water temperature. Sea height changes at tidal and seasonal periods have been observed to regulate methane plume activity (Riedel et al., 2018). Shorter term patterns may also be associated with brief periods of excitement of local methane seeps.

Further work could be done to understand the distribution possible mechanism of SDEs in the CI data. If the SDEs were detected using a short-term to long-term RMS trigger, then their rates could be quantified, and it could be determined whether they are present on all OBSs at some level. The rate of SDEs could be examined as a function of time of day, and the presence of daylight, dusk, and dawn for correlations that might be indicative of a biological signal, or as function of tide height which might be indicative of a gas related mechanism. Batsi et al. (2019) inferred that gas-generated SDEs are linked to the presence of cold seeps or a bottom simulating reflector (BSR). For the CI data, the distribution of the bottom simulating reflector and known sites of gas venting could be compared with variations in the intensity of SDEs. We note that more methane cold seeps have been identified in the Grays Harbor region than the Cape Mendocino region (Johnson et al., 2019; Riedel et al., 2018) which is consistent with variations in the mean to median ratio, but this difference in the number of seeps may just reflect the relative paucity of surveys for methane plumes off northern California. One way to demonstrate that SDEs are not related to biological activity would be to show that they are not recorded on buried sensors. Unfortunately, all the buried sensors on the Northeast Pacific Ocean cabled observatories are at ocean depths deeper than those where SDEs are a dominant source of noise. Since bubble plumes have been observed to have characteristic noise at ~10 kHz (Bergès et al., 2015), another possibility would be to deploy instruments with higher sampling rate hydrophones to record events to determine where SDEs are associated with bubble plume signals. Perhaps, the only conclusive way to demonstrate or discount a biological origin for bio-bumps may be to repeat the camera studies of Batsi et al. (2019) in a wider range of water depths although this would itself be challenging for shielded instruments.

5. Conclusions

We have analyzed noise recorded by OBSs in the 5–12 Hz band for the 2013–2014 and 2014–2015 deployments of the Cascadia Initiative experiment. Noise levels vary substantially between sites and instrument types at all depths but are generally found to be highest on the continental shelf (<~200 m depth) and lowest on deep ocean instruments (>2,500 m depth) that are over 100 km from the base of the continental slope. On the inner continental shelf, the primary continuous noise source arises from the orbital motions of ocean waves. In the deep ocean, wind-generated ocean spray noise is observed on the quietest instruments at wind speeds of >~10 m/s. Elsewhere the noise on CI OBSs is dominated by ocean bottom currents. The bottom currents timeseries predicted by a regional ocean circulation model are not sufficiently accurate to model the noise at specific CI sites but in concert with limited measurements of bottom currents, the circulation model is useful for understanding the spatial variability and depth dependence of currents. Mean bottom currents and median noise levels can vary substantially between different sites at any given depth but on average tend to decrease with increasing depth on the continental slope and with distance away from the base of the slope on the abyssal plane.

There are clear differences in the noise performance of the different OBS designs used in the Cascadia experiment which are consistent with shorter instruments and instruments with a smooth profile having lower high-frequency noise levels. We infer that noise is generated by turbulence over the whole instrument rather than just the sensor and that shielding may not reduce noise in this frequency band. Ideally the sensor should be buried to eliminate current noise but for instruments that sit on the seafloor a design with a low hydrodynamic profile is optimal.

Non-earthquake short-duration events were identified as a major source of intermittent noise on many OBSs on and near the continental shelf by looking time series of the ratio noise based on a mean and a median. Further analysis and experimentation will be required to determine whether these signals are more consistent with biological source or with gas bubble movements in the subseafloor.

Data Availability Statement

Data used in this research were provided by instruments from the Ocean Bottom Seismograph Instrument Pool (http://www.obsip.org) which is funded by the National Science Foundation. OBSIP data are archived at the IRIS Data Management Center (http://www.iris.edu). Weather hindcast data used in this research were provided by the National Oceanic and Atmospheric Administration Wavewatch III production hindcast archived by the NOAA Environmental Modeling Center (https://polar.ncep.noaa.gov). Current prediction data used in this research were provided by the LiveOcean Pacific Northwest Ocean and Estuary Forecast produced by the University of Washington Coastal Modeling Group (https://faculty.washington.edu/pmacc/LO/LiveOcean.html).

Acknowledgments

We thank Paul Johnson, Parker MacCready, and Emily Roland for helpful discussions and comments. We also thank Louis Géli and two anonymous referees for thorough reviews. Funding for this work was provided through Grant GBMF5231 from the Gordon and Betty Moore Foundation, and the Jerome M. Paros Chair in Sensor Networks.

References

Alford, M., Mickett, J., Zhang, S., MacCready, P., Zhao, Z., & Newton, J. (2012). Internal waves on the Washington continental shelf. *Oceanography*, *25*(2), 66–79. https://doi.org/10.5670/oceanog.2012.43

Ardhuin, F., Gualtieri, L., & Stutzmann, E. (2015). How ocean waves rock the Earth: Two mechanisms explain microseisms with periods 3 to 300 s. *Geophysical Research Letters*, *42*, 765–772. https://doi.org/10.1002/2014GL062782

Batsi, E., Tsang-Hin-Sun, E., Klingelhoefer, F., Bayrakci, G., Chang, E. T. Y., Lin, J., et al. (2019). Nonseismic signals in the ocean: Indicators of deep sea and seafloor processes on ocean-bottom seismometer data. *Geochemistry, Geophysics, Geosystems*, *20*, 3882–3900. https://doi.org/10.1029/2019GC008349

Bell, S. W., Forsyth, D. W., & Ruan, Y. (2015). Removing noise from the vertical component records of ocean-bottom seismometers: Results from year one of the Cascadia Initiative. *Bulletin of the Seismological Society of America*, *105*, 300–313. https://doi.org/10.1785/0120140054

Bergès, B. J. P., Leighton, T. G., & White, P. R. (2015). Passive acoustic quantification of gas fluxes during controlled gas release experiments. *International Journal of Greenhouse Gas Control*, *38*, 64–79. https://doi.org/10.1016/j.ijggc.2015.02.008

Boegman, L., & Stastna, M. (2019). Sediment resuspension and transport by internal solitary waves. *Annual Review of Fluid Mechanics*, *51*, 129–154. https://doi.org/10.1146/annurev-fluid-122316-045049

Bowman, D. C., & Wilcock, W. S. D. (2014). Unusual signals recorded by ocean bottom seismometers in the flooded caldera of Deception Island volcano: Volcanic gases or biological activity? *Antarctic Science*, *26*, 267–275. https://doi.org/10.1017/S0954102013000758

Buskirk, R. E., Frohlich, C., Latham, G. V., Lawton, J., & Chen, A. T. (1981). Evidence that biological activity affects ocean bottom seismograph recordings. *Marine Geophysical Research*, *5*(2), 189–205.

Collins, J. A., Vernon, F. L., Orcutt, J. A., Stephen, R. A., Peal, K. R., Wooding, F. B., et al. (2001). Broadband seismology in the oceans: Lessons from the ocean seismic network pilot experiment. *Geophysical Research Letters*, *28*(1), 49–52. https://doi.org/10.1029/2000GL011638

Crawford, W. C., & Webb, S. C. (2000). Identifying and removing tilt noise from low-frequency (<0.1 Hz) seafloor vertical seismic data. *Bulletin of the Seismological Society of America*, *90*(4), 952–963. https://doi.org/10.1785/0119990121

Csanady, G. T. (1988). Ocean currents over the continental slope. *Advances in Geophysics*, *30*, 95–203. https://doi.org/10.1016/S0065-2687(08)60421-5

Dozorov, T. A., & Soloviev, S. L. (1991). Spectra of ocean-bottom seismic noise in the 0.01–10 Hz range. *Geophysical Journal International*, *106*(1), 113–121. https://doi.org/10.1111/j.1365-246X.1991.tb04605.x

Duennebier, F. K., & Sutton, G. H. (1995). Fidelity of ocean bottom seismic observations. *Marine Geophysical Researches*, *17*(6), 535–555. https://doi.org/10.1007/BF01204343

Duennebier, F. K., McCreery, C. S., Harris, D., Cessaro, R. K., Fisher, C., & Anderson, P. (1987). OSS IV: Noise levels, signal to noise ratios, and noise sources. *Deep Sea Drilling Project Initial Reports*, *88*, 89–103.

Dunn, R. A., & Hernandez, O. (2009). Tracking blue whales in the eastern tropical Pacific with an ocean-bottom seismometer and hydrophone array. *The Journal of the Acoustical Society of America*, *126*(3), 1084–1094. https://doi.org/10.1121/1.3158929

Dyer, K. R. (1986). *Coastal and estuarine sediment dynamics*. Chichester; New York: Wiley.

Ewing, J., & Ewing, M. (1961). A telemetering ocean-bottom seismograph. *Journal of Geophysical Research*, *66*(11), 3863–3878. https://doi.org/10.1029/JZ066i011p03863

Francis, T. J. G., Porter, I. T., Lane, R. D., Osborne, P. J., Pooley, J. E., & Tomkins, P. K. (1975). Ocean bottom seismograph. *Marine Geophysical Research*, *2*(3), 195–213. https://doi.org/10.1007/BF00305503

Frontera, T., Ugalde, A., Olivera, C., Jara, J. A., & Goula, X. (2010). Seismic ambient noise characterization of a new permanent broadband ocean bottom seismometer site offshore Catalonia (Northeastern Iberian Peninsula). *Seismological Research Letters*, *81*(5), 740–749. https://doi.org/10.1785/gssrl.81.5.740

Giddings, S. N., MacCready, P., Hickey, B. M., Banas, N. S., Davis, K. A., Siedlecki, S. A., et al. (2014). Hindcasts of potential harmful algal bloom transport pathways on the Pacific Northwest coast. *Journal of Geophysical Research: Oceanography*, *119*, 2439–2461. https://doi.org/10.1002/2013JC009622

Godin, O. A., & Chapman, D. M. F. (1999). Shear-speed gradients and ocean seismo-acoustic noise resonances. *The Journal of the Acoustical Society of America*, *106*(5), 2367–2382. https://doi.org/10.1121/1.428074

Hasselmann, K. (1963). A statistical analysis of the generation of microseisms. *Reviews of Geophysics*, *1*(2), 177–210. https://doi.org/10.1029/RG001i002p00177

Hayes, S. P. (1980). The bottom boundary layer in the eastern tropical Pacific. *Journal of Physical Oceanography*, *10*(3), 315–329. https://doi.org/10.1175/1520-0485(1980)010<0315:TBBLIT>2.0.CO;2

Johnson, H. P., Merle, S., Salmi, M., Embley, R., Sampaga, E., & Lee, M. (2019). Anomalous concentration of methane emissions at the continental shelf edge of the northern Cascadia Margin. *Journal of Geophysical Research: Solid Earth*, *124*, 2829–2843. https://doi.org/10.1029/2018JB016453

Juan, C., Van Rooij, D., & De Bruycker, W. (2018). An assessment of bottom current controlled sedimentation in Pacific Ocean abyssal environments. *Marine Geology*, *403*, 20–33. https://doi.org/10.1016/j.margeo.2018.05.001

Keulegan, G. H. (1938). Laws of turbulent flow in open channels. *Journal of Research of the National Bureau of Standards*, *21*(6), 707–741. https://doi.org/10.6028/jres.021.039

Longuet-Higgins, M. S. (1950). A theory of the origin of microseisms. *Philosophical Transactions of the Royal Society of London. Series A, Mathematical and Physical Sciences*, *243*(857), 1–35.

MacCready, P., & Giddings, S. N. (2016). The mechanical energy budget of a regional ocean model. *Journal of Physical Oceanography*, *46*, 2719–2733. https://doi.org/10.1175/JPO-D-16-0086.1

McCreery, C. S., Duennebier, F. K., & Sutton, G. H. (1993). Correlation of deep ocean noise (0.4–30 Hz) with wind, and the Holu Spectrum—A worldwide constant. *The Journal of the Acoustical Society of America*, *93*(5), 2639–2648. https://doi.org/10.1121/1.405838

Montagner, J.-P., Karczewski, J.-F., Romanowicz, B., Bouaricha, S., Lognonne, P., Roult, G., et al. (1994). The French pilot experiment OFM-SISMOBS: First scientific results on noise level and event detection. *Physics of the Earth and Planetary Interiors*, *84*(1–4), 321–336. https://doi.org/10.1016/0031-9201(94)90050-7

Pillet, R., Deschamps, A., Legrand, D., Virieux, J., Béthoux, N., & Yates, B. (2009). Interpretation of broadband ocean-bottom seismometer horizontal data seismic background noise. *Bulletin of the Seismological Society of America*, *99*(2B), 1333–1342. https://doi.org/10.1785/0120080123

Riedel, M., Scherwath, M., Römer, M., Veloso, M., Heesemann, M., & Spence, G. D. (2018). Distributed natural gas venting offshore along the Cascadia margin. *Nature Communications*, *9*, 3264. https://doi.org/10.1038/S51467-018-05736-x

Romanowicz, B., Stakes, D., Dolenc, D., Neuhauser, D., McGill, P., Uhrhammer, R., & Ramirez, T. (2006). The Monterey Bay broadband ocean bottom seismic observatory. *Annals of Geophysics*, *49*(2–3), 607–623.

Stähler, S. C., Panning, M. P., Vance, S. D., Lorenz, R. D., van Driel, M., Nissen-Meyer, T., & Kedar, S. (2018). Seismic wave propagation in icy ocean worlds. *Journal of Geophysical Research: Planets*, *123*, 206–232. https://doi.org/10.1002/2017JE005338

Stakes, D., McClain, J., VanZandt, T., McGill, P., & Begnaud, M. (1998). Corehole seismometer development for low-noise seismic data in a long-term seafloor observatory. *Geophysical Research Letters*, *25*(14), 2745–2748. https://doi.org/10.1029/98GL01937

Sutton, G. H., McDonald, W. G., Prentiss, D. D., & Thanos, S. N. (1965). Ocean-bottom seismic observatories. *Proceedings of the IEEE*, *53*(12), 1909–1921. https://doi.org/10.1109/PROC.1965.4468

Tary, J. B., Géli, L., Guennou, C., Henry, P., Sultan, N., Çağatay, N., & Vidal, V. (2012). Microevents produced by gas migration and expulsion at the seabed: A study based on sea bottom recordings from the Sea of Marmara: Microevents produced by gas migration. *Geophysical Journal International*, *190*(2), 993–1007. https://doi.org/10.1111/j.1365-246X.2012.05533.x

Tolman, H. L. (1989). The numerical model WAVEWATCH: A third generation model for the hindcasting of wind waves on tides in shelf seas. *Communications on Hydraulic and Geotechnical Engineering*, Delft Univ. of Techn., ISSN 0169–6548, Rep. no. 89–2, 72 pp.

Tolman, H. L. (2006). Development of a multi-grid version of WAVEWATCH III. NOAA/NWS/NCEP/MMAB Technical Note 256, 88 pp.+ Appendices.

Toomey, D., Allen, R., Barclay, A., Bell, S., Bromirski, P., Carlson, R., et al. (2014). The Cascadia Initiative: A sea change in seismological studies of Subduction zones. *Oceanography*, *27*, 138–150. https://doi.org/10.5670/oceanog.2014.49

Trehu, A. (1985). A note on the effect of bottom currents on an ocean bottom seismometer. *Bulletin of the Seismological Society of America*, *75*(4), 1195–1204.

Trehu, A. M., & Sutton, G. H. (1994). A note on the seafloor coupling characteristics of the new ONR ocean-bottom seismometer. *Marine Geophysical Researches*, *16*(2), 91–103. https://doi.org/10.1007/bf01224755

Webb, S. C. (1998). Broadband seismology and noise under the ocean. *Reviews of Geophysics*, *36*(1), 105–142. https://doi.org/10.1029/97RG02287

Webb, S. C., & Crawford, W. C. (2010). Shallow-water broadband OBS seismology shallow-water broadband OBS seismology. *Bulletin of the Seismological Society of America*, *100*(4), 1770–1778. https://doi.org/10.1785/0120090203

Weirathmueller, M. J., Stafford, K. M., Wilcock, W. S., Hilmo, R. S., Dziak, R. P., & Tréhu, A. M. (2017). Spatial and temporal trends in fin whale vocalizations recorded in the NE Pacific Ocean between 2003–2013. *PLoS ONE*, *12*, e0186127. https://doi.org/10.1371/journal.pone.0186127

Wiegel, R. L., & Johnson, J. W. (1950). Elements of wave theory. *Coastal Engineering Proceedings*, *1*, 5–21. https://doi.org/10.9753/icce.v1.2

Wilcock, W. S. D., Webb, S. C., & Bjarnason, I. T. (1999). The effect of local wind on seismic noise near 1 Hz at the MELT site and in Iceland. *Bulletin of the Seismological Society of America*, *89*(6), 1543–1557.

Williams, M. C., Tréhu, A. M., & Braunmiller, J. (2010). Local earthquake detection in marine environments using seismic signal parameters, S53A-1965, poster presented at 2010 Fall AGU meeting.

Xie, X., Liu, Q., Zhao, Z., Shang, X., Cai, S., Wang, D., & Chen, D. (2018). Deep sea currents driven by breaking internal tides on the continental slope. *Geophysical Research Letters*, *45*, 6160–6166. https://doi.org/10.1029/2018GL078372

Yttervik, R., & Furnes, G. K. (2005). Current measurements on the continental slope west of Norway in an area with a pronounced two-layer density profile. *Deep Sea Research Part I: Oceanographic Research Papers*, *52*(1), 161–178. https://doi.org/10.1016/j.dsr.2004.08.011